Macromolecules

pubs.acs.org/Macromolecules Article

Ionic Liquid Enhanced Parallel Lamellar Ordering in Block Copolymer Films

Ali Masud, Melanie Longanecker, Sonal Bhadauriya, Maninderjeet Singh, Wenjie Wu, Kshitij Sharma, Tanguy Terlier, Abdullah M. Al-Enizi, Sushil Satija, Jack F. Douglas,* and Alamgir Karim*

Cite This: *Macromolecules* 2021, 54, 4531−4545 Read Online

ACCESS | Metrics & More | Article Recommendations | Supporting Information

ABSTRACT: Previous studies have shown that the degree of ordering and alignment in block copolymer (BCP) films can be enhanced by increasing the thermodynamic driving force for microphase separation, χN, where χ is the Flory−Huggins interaction parameter between the polymer components and N is the number of statistical segments in the BCP. In practice, this strategy for controlling the microstructure of any BCP film normally involves reducing the temperature T and/or increasing N. However, both of these methods have the drawback of leading to a corresponding slowing down of the rate of ordering and dynamic-heterogeneity-associated defect formation in the material, related to both glass formation and entanglement. In the present work, we explore the use of an ionic liquid (IL) having a high cohesive interaction strength with a relatively low volatility to increase the cohesive interaction parameter χ, while at the same time keeping the molecular mobility high. In particular, we show that IL-driven enhancement of χ and higher molecular mobility, coupled with the poly(methyl methacrylate) (PMMA) surface wetting interaction strength, induces enhanced substrate-driven stratification of parallel lamellae in polystyrene-*b*-poly(methyl methacrylate) BCP (PS−PMMA) films over much larger distances than without IL. We anticipate that this method can be used to prepare relatively defect-free multilayer films wherein the IL is mostly removed under vacuum annealing during the short processing time while preserving the intrinsic lamellar morphology despite the initial high-IL mass fraction. This approach should be extremely useful in applications like barrier materials and batteries, solid-state dielectric capacitors, optical waveguides, and other applications where substrate-parallel multilayer films of controlled thickness are required.

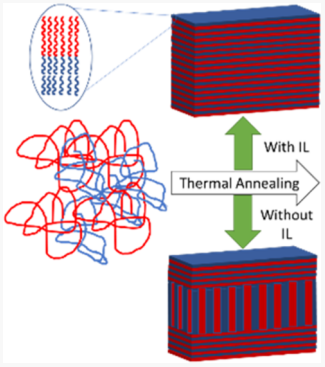

INTRODUCTION

Block copolymers (BCPs) have garnered attention for their ability to form small periodic features with dimensions ranging from 5 nm to as large as 100 nm.[1,2] Contrast for nanotech applications is developed by having two polymers covalently bonded at a molecular scale, in conjunction with microphase separation between these polymer "blocks" having different chemistries to create ordered BCP morphologies. Well-ordered and well-oriented BCPs have been applied to develop numerous useful new materials, and we mention a few applications for specific illustration: capacitors,[3] lithium-ion batteries,[4] photonics,[5] separation membranes,[6] nanolithographic templates,[7] precursor for quantum dot arrays,[8] nanocrystal flash memory,[8] nanowire array field-effect transistor (FET),[8] etc. In the present work, we are concerned with the formation of ordered BCP morphologies (e.g., spherical, cylindrical, lamellar, or some combination of these structures[9]) in thin films using ionic liquid (IL) as an enabler for directed self-assembly (DSA). Of particular interest for the present work is ordering and orientation control of lamellae-forming BCPs having relatively higher molecular mass M_w and large lamellae thickness.

Several DSA methods have been utilized to control the ordering of BCP materials, such as thermal annealing,[10] zone annealing,[3] topographical and chemical patterning,[11,12] soft shear,[13] solvent annealing,[14] electric field,[15] and laser field alignment.[15] Most of these methods have their own benefits and drawbacks; however, thermal annealing remains one of the most versatile and readily adoptable methods for many current industrial applications,[8] and thus has been chosen as the DSA method in this work. Many applications have focused on the use of relatively symmetric BCPs of polystyrene-*b*-poly(methyl methacrylate) (PS−PMMA), which form a lamellar structure. Bare silicon surfaces normally have a thin layer of native SiO_2, and alternating layers of PMMA and PS lamellae form near the surfaces due to the preferential affinity of the PMMA block to the SiO_2 substrate and PS to air. The domain length periodicity of the alternating layer equals L_o, but the parallel registry of these patterns leads to a damped compositional profile emanating from the substrate that normally extends up to a thickness $h \leq 6L_o$ for $M_w < 70k$.[8,16] This defines a

Received: November 18, 2020
Revised: April 4, 2021
Published: May 6, 2021

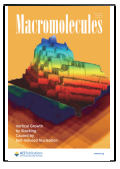

https://doi.org/10.1021/acs.macromol.0c02546
Macromolecules 2021, 54, 4531−4545

correlation length describing the spatial range over which the substrate exerts orientational correlation of the BCP lamellae via PMMA interaction with the film substrate. A similar effect, with a smaller correlation length, arises at the air surface due to the lower surface energy of the PS block. The molecular and processing factors that control this important substrate-and-air interface-directed correlation scale are currently largely unknown, but we anticipate that a greater driving force for microphase separation and higher mobility in the film before the film vitrifies should lead to a larger correlation length important to applications. Our measurements below confirm these general expectations.

In the case of low-molecular-mass BCP films with a high Flory−Huggins interaction parameter, χ, highly parallel ordered layers throughout the film thickness have been observed.[17] However, in the case of modestly high M_w PS−PMMA block copolymer films, given the χ between blocks is relatively small, the length scale over which the BCP remains correlated in the parallel orientation from the surface is relatively small and strongly damped in the block compositional amplitude,[18] which is the problem the present paper addresses. We also note that for "sufficiently thin" ($<5L_o$) films, the parallel lamellar layering is "directed" from both the air and substrate interfaces,[16] leading to essentially complete layering within the film, a finite size effect, observed for BCP films, both below and above the film ODT.[3,19−21] If the film thickness h is an exact half-integer multiple of the number of layers (n) and L_o, then the film surface satisfies a commensurate condition leading to smooth interfaces.[22] The top air and the bottom silicon surface each form a $1/2L_o$ layer of PS and PMMA, respectively. However, for incommensurate thicknesses, $h \neq (n + 1/2)L_o$, surface structure in the form of islands and holes arises with depth on the order of L_o, measurable using atomic force microscopy (AFM).[22] It is evidently then of interest to increase the correlation length of the lamellae orientation with the substrate by increasing the strength of the thermodynamic driving force for microphase separation, χN, in order for the thickness of this type of highly aligned block copolymer films to increase for reliable application of such films that requires many layers, e.g., increasing the resistance of polymer films to dielectric breakdown,[3] reduction of gas permeability, etc.

Ionic liquids (ILs) have received a lot of attention for their potential in environmentally friendly processing of polymer materials,[23,24] and a high cohesive energy is characteristic of these materials, making them an obvious choice for the present study seeking enhanced substrate-induced lamellae orientation of BCPs in thin films. ILs have already found applications in many areas in polymer science, such as in the synthesis of polymer electrolytes for batteries, membranes, fuel cells, etc.[23] In block copolymers (BCPs), such as PS-PMMA, certain ILs have been found to preferentially segregate to the polar PMMA block, enhancing the mobility of this block, much like an uncharged plasticizer additive,[25] while at the same time enhancing χ.[26−28] Bennet et al. used IL,[26] such as (EMIM NTF_2), to show that they can enhance χ, thus inducing order in low χN films, and that it has affinity to the PMMA block and decreases the glass-transition temperature T_g of the BCP.[26] Earlier, Yamamuro et al. found that the IL (1-ethyl-3-methylimidazolium bis(trifluoromethylsulfonyl)imide (EMIM TFSI)) utilized in the present work greatly reduced the glass transition temperature of PMMA.[29] More recently, Chen et al. further demonstrated that a low M_w (N) BCP with IL can attain pitches below 20 nm.[28] We may then anticipate that the IL satisfies the two essential design requirements: enhanced cohesive energy density of the PMMA block in the BCP and thus enhanced immiscibility with the PS block, while lowering the T_g of the PMMA block for enhanced molecular mobility.

We previously systematically explored the enhancement of BCP ordering in films through the increase of the BCP molecular mass[30] and decreasing temperature.[10] Earlier, we had shown that IL (EMIM TFSI) can enhance the processing window for attaining a perpendicular cylinder orientation due to the change in surface tension and segmental relaxation.[31] Interestingly, IL has a relatively low surface tension despite the relatively high cohesive interaction strength, which alters the BCP wetting characteristics.[31] Russell and co-workers earlier showed that adding lithium salts to PS−PMMA block copolymer materials increases χN[32] when there is a selective affinity of the ionic species for the polar PMMA block. The approach of using ILs to enhance the ordering and orientation of BCP mesophases, through modifying χN, is clearly quite promising since these additives offer a synergy of positive effects for efficient processing as well as an enhanced range of BCP ordering.

In the present contribution, we demonstrate several enhancements uniquely with a controlled amount of IL additive, over only traditional thermal annealing for parallel ordering, resulting in long-range ordering of the PS−PMMA lamellar system. The addition of IL has several synergistic effects that enhance parallel ordering: (1) lowering of T_g of the PMMA block, and thereby of the BCP film average, allowing for much faster kinetics, especially as applied to high M_w BCP systems; (2) increase of χ between the IL-wetted PMMA block and the PS block, leading to a sharper interface, and resulting in a much longer range propagation into the film interior of parallel lamellae from the silicon substrate wetted by the PMMA block (a broad BCP interface dampens the correlation length); (3) despite the initial addition of significant ILs (up to 40 wt %), the final morphology remains the intrinsic BCP lamellar structure, rather than nonlamellar, due to the important finding, i.e., (4) self-removal of ≈99% of the IL under vacuum annealing during and upon completion of the rapid ordering, a process beneficial both for the environment, and T_g enhancement leading to enhanced mechanical properties at the end of the ordering process. The volatility of ionic liquids at reduced pressure was reported earlier by Earle et al.,[33] forming an important processing advantage was exploited in this paper.

Specifically, we show that in the lamellar PS-PMMA system, long-range parallel ordering is induced for significantly higher M_w and over a much higher film thickness regime than previously obtained. Notably, both of these are very difficult to obtain by thermal annealing alone. We demonstrate this phenomenon in BCP films containing IL, up to 750 nm ($\approx 20L_o$) in thickness, and with high molecular masses (≈127.5k), using traditional vacuum thermal annealing in relatively short time scales. Such a high degree of ordering and correlation length of substrate and air-interface-directed correlational orientation is not achievable in the same neat BCP films without the added IL. Recent measurements by Runt and co-workers have shown that the addition of ionic species to polymer materials of interest in battery applications leads to a significant enhancement of mobility in these materials associated with the reduction of the fragility of glass formation.[34] It appears from our measurements that the utilization of an ionic fluid as a solvent for our block copolymer

https://doi.org/10.1021/acs.macromol.0c02546
Macromolecules 2021, 54, 4531−4545

likewise increases the molecular mobility in the temperature range in which we process our films, although we do not quantitatively estimate the relaxation time of the cast films in the present work. Further, these films exhibit the traditional formation of islands and holes, as occurs in fully ordered lamellar BCP films. We exploit this phenomenon to reveal and correlate the surface island and hole formation with the internal parallel lamellae ordering profile development in the BCP film. Our approach involves tracking the incremental increase of island/hole height with an increase of the IL content by AFM, in its approach from sub-L_o to L_o scales, which quantifies the formation of parallel lamellar structure in the BCP film.

EXPERIMENTAL SECTION

Film Preparation and Processing. Symmetric diblock copolymer of PS−PMMA (L-BCP) of different molecular masses of 66k (33k−3k) and 127.5k (65k−62.5k), deuterated PS−PMMA (dPS−PMMA) of 19.5k−18.1k, 29.5k−32.5k, and 47.5k−51k, and PMMA homopolymer of 30k were purchased from Polymer Source Inc. having a very low polydispersity index (PDI) of 1.07−1.1. The polymers were dissolved in a toluene and tetrahydrofuran (THF) mixture to form a 4−8 mass % by volume of solution. The ionic liquid 1-ethyl-3-methylimidazolium bis(trifluoromethylsulfonyl) imide ([EMIM][TFSI]), purchased from TCI Chemicals[35] with greater than 98% purity, was dissolved in THF and added to the polymer solution in different proportions. The polymer was then filtered using a syringe and a 0.2 μm filter. The polymer was flow-coated into a film at 2−4 cm/s on a Si(100) wafer purchased from University Wafer, using a 2−4 mass % BCP solution with IL. Prior to casting, the silicon wafer was cleaned using a chemical wash and UV-treated for 2 h to remove any contaminants prior to film deposition. The films were then dried for 24 h in vacuum at 60 °C to remove any residual toluene or THF. The thicknesses of the film were then measured on Filmetrics F3UV correct to a resolution of 1 nm. The films were then thermally annealed (TA) in a vacuum seal between 170 and 240 °C for a period of 8 h to up to 2 days.

Characterization. Topography images of the thermally annealed samples were measured using AFM in the tapping mode. The Bruker AXS Dimension Icon was used in these measurements. Optical microscope images were collected using an Olympus CX 43 microscope. Grazing-incidence small-angle X-ray scattering (GISAXS) was performed at the Advanced Photon Source of the Argonne National Lab, on beamline 8-ID-E40. X-ray with a photon energy of 7.35 keV and a wavelength of λ = 1.6868 Å was impinged on the sample at a grazing angle of 0.1−0.2°. It is known that the critical angles of the film and the silicon wafer are 0.11 and 0.16, respectively. The best intensity for through-thickness penetration was found at an incident angle of 0.14, and it probes the bulk of the film. The reflected waves were detected on a Dectris Pilatus 1M pixel-array detector. An Argonne-developed software called GIXSGUI was used to convert the data to the q space and draw line-spaces to obtain the scattering intensity I as a function of the wave vector q.[36]

Positive and negative high-mass-resolution depth profile was performed using a time-of-flight secondary ion mass spectrometry (ToF-SIMS) NCS instrument, which combines a ToF-SIMS5 instrument (ION-ToF GmbH, Münster, Germany) and an in situ scanning probe microscope (NanoScan, Switzerland). A bunched 30 keV Bi_3^+ ion (with a measured current of 0.02 pA) was used as the primary probe for analysis (scanned area 100 × 100 μm^2), and sputtering was performed using Ar_{1500}^+ ions at 10 keV with a typical current around 0.3 nA, where the rastered region has an area of 500 × 500 μm^2. The beams were operated in the noninterlaced mode, alternating between one analysis cycle and one sputtering cycle (corresponding to 1.63 s), followed by a pause of 3 s for charge compensation with an electron flood gun. An adjustment of the charge effects has been operated using a surface potential of −8 V and an extraction bias of 0 V. During depth profiling, the cycle time was fixed at 200 μs, corresponding to 0−3644 atomic mass units (m/z).

The NIST Center for Neutron Research NG 7 reflectometer was used for the neutron reflectivity (NR) measurements. The neutron beam was collimated to 4.76 Å wavelength at a constant source and 0.18 Å divergence used in the emitter. The magnitude of the wave vector (Q_z) was calculated using $Q_z = 4\pi \sin(\theta)/\lambda$, where λ is the wavelength and θ is the angle of incidence with a range of 0.006−0.16 $Å^{-1}$. The data were reduced using ReflRed software and analyzed and fitted using Reflpak software.[37]

RESULTS AND DISCUSSION

The essential premise of our present study is to investigate how and by what mechanisms an ionic liquid (IL) impacts the degree of parallel alignment of PS−PMMA lamellae-forming block copolymer films on silicon surfaces. In this regard, we do not investigate relatively low-molecular-mass PS−PMMA (M_w < 50k total) since they naturally order to produce highly aligned parallel lamellae with thermal annealing even in thick films (up to several micrometers, provided that the annealing temperature is optimized, substrate wetting is strong, and sufficient time is allowed for defect annihilation).[3,38,39] Rather, we investigate how IL impacts the processing to produce parallel layering in thicker high-molecular-mass PS−PMMA films, which otherwise do not exhibit good parallel lamellar ordering with thermal annealing. Two different L-BCP PS−PMMA systems investigated are a relatively intermediate M_w and a high M_w system: 33k−33k (66k) and 65k−62.5k (127.5k) with the film thickness ranging from 200 to 750 nm. As the diffusion coefficient scales with molecular mass as M_w^{-2}, the diffusion coefficient for the neat higher 128k M_w system is ≈4 times lower than that of the neat 66k system, making it extremely difficult to order well on practical time scales. Enhancements in the ordering kinetics and substrate-parallel layering of IL-containing PS−PMMA films from each polymer system at different thicknesses are discussed below.

Intermediate M_w PS−PMMA (33k−33k, M_w = 66k). Neat PS−PMMA of total M_w between 25k and 50k forms parallel lamellae readily with thermal annealing. This is because the product *of* χN (>10.5) is large enough to induce microphase separation, and the system has a high mobility (high diffusion coefficient). For higher molecular masses, far above the entanglement molecular mass, M_e (PS ≈ 13k; PMMA ≈ 10k),[40] it becomes increasingly more difficult to order and substrate-align the BCPs.[41] In practice, for symmetric PS−PMMA BCPs, with M_w > 70k and film thickness h > 200 nm (above $6L_o$), attaining complete parallel ordering without any nonparallel "fingerprint-like" meandering of lamellae in the lamellar PS−PMMA system on bare silicon is elusive. This is due to factors such as reduced diffusivity, lower surface energy differential, and the low Flory−Huggins interaction parameter of the PS−PMMA block copolymer system. It is well-understood that drivers for phase separation in the BCP system include a larger Flory−Huggins interaction parameter (χ) and number of monomers (N) in the polymer backbone. The higher the product of χN, the higher is the degree of phase separation.[9] As the blocks' M_w increases, diffusive motion decreases and the surface energy differential driving force is insufficient to propagate the overlap of ordered lamellar layers from both interfaces into the interior of thick films in practical annealing time frames, and consequently the lamellae start to meander, which is the most prevalent in the middle of the film.[16,20,42] These randomly oriented layers may hinder the application of BCPs in important applications such

https://doi.org/10.1021/acs.macromol.0c02546
Macromolecules 2021, 54, 4531−4545

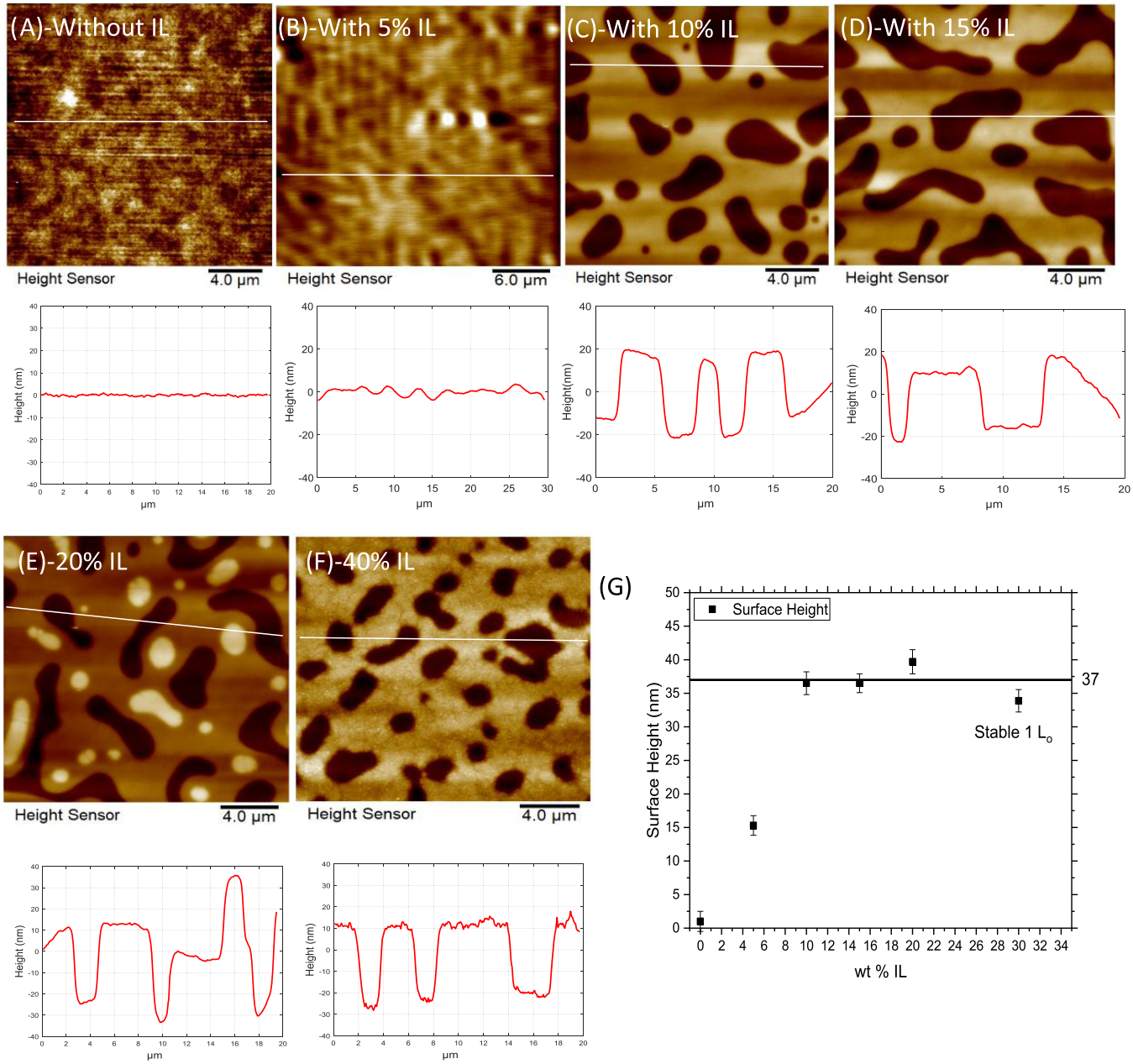

Figure 1. AFM morphology with line-cuts of the PS-*b*-PMMA 33k−33k ordered using TA at 170 °C for 9 h for thicknesses of about 210−230 nm: (A) no IL and by mass relative to the BCP mass of the casting solution:(B) 5% IL, (C) 10% IL, (D) 15% IL, (E) 20% IL, and (F) 40% IL. (G) Evolution of morphology on the surface for lamellar systems from the AFM height profile as the amount of IL increases. The lamellar ordering, inferred from the fidelity of island and hole formation, is optimal at 10% IL. The uncertainty measurements were taken from the standard deviation from few average values of the AFM line-cut profile.

as optoelectronic devices, capacitors,[43] lithium-ion batteries, etc.[22,24]

As the M_w and film thickness increase, the temperature and time of ordering of BCPs above the glass-transition temperature to attain ordering can increase exponentially. Diffusivity of the segments decreases exponentially with an increase in the degree of polymerization, N, i.e., $D \sim \exp(-\alpha\chi N)$, by the Roults approximation,[44] where a is the statistical segmental length and χ progressively decreases with the thermal annealing temperature above the glass-transition temperature. Local BCP ordering and alignment of PS−PMMA become increasingly difficult with increasing BCP mass and lowered T. Several methods have been explored in the literature to enhance the formation of the parallel lamellae and inhibit the formation of perpendicular lamellae through films, for example, the use of preferential top and bottom layer coating,[16,45] solvent-based ordering to enhance mobility of the blocks,[2,46] nanoparticle[47]-based ordering, etc. Preferential coating may involve placing a PS or PMMA or a neutral layer on the substrate surface or above the film surface. Depending on the surface energy differential, a lamellar PS−PMMA can self-assemble into parallel or perpendicular lamellae upon thermal annealing.[48−50] While surface energy modification is an additional control parameter to control BCP orientation within the surface-directed range ($h \approx 6L_o$), it cannot still solve the problem of inducing a higher degree, as measured by

https://doi.org/10.1021/acs.macromol.0c02546
Macromolecules 2021, 54, 4531−4545

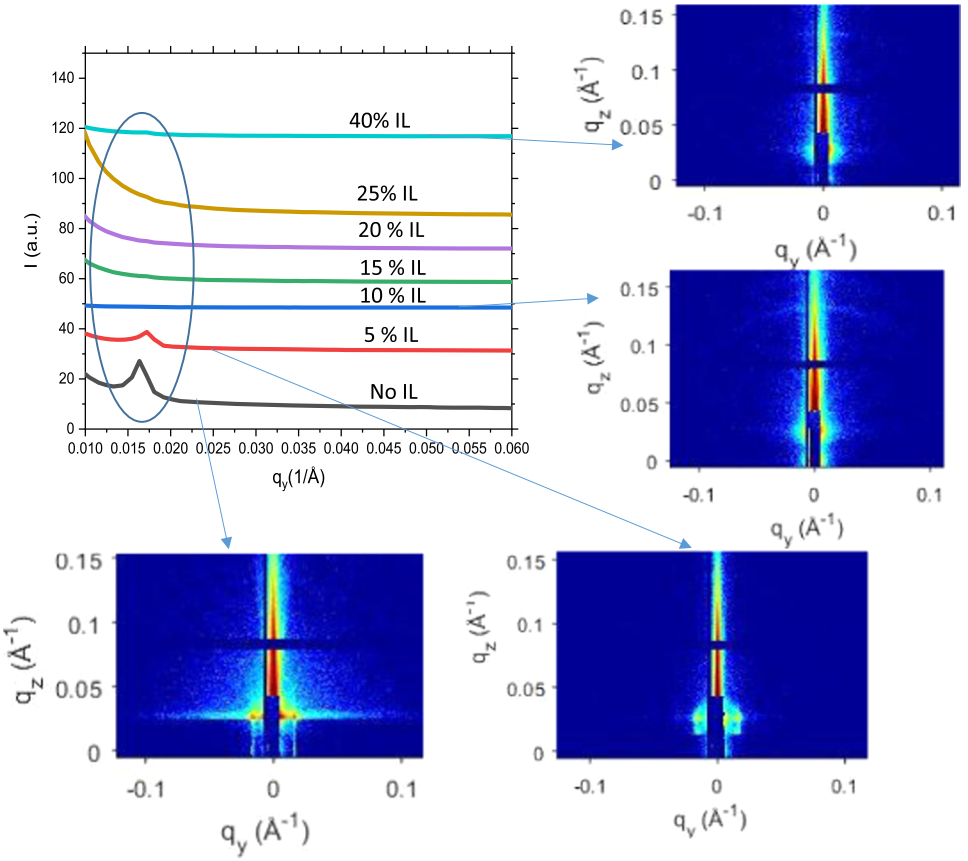

Figure 2. GISAXS line-cut profile obtained from taking the cumulative q_y along all q_z. The images corresponding to the line-cuts at different ILs are seen in the figure as well. Note that the Bragg peak in the image has disappeared as the IL increases.

the increased correlation length, or complete through-thickness parallel orientation in PS-PMMA lamellar films at higher M_w and higher thickness limits.[16]

The in-plane (nonparallel) meandering of L-BCP lamellae (that can be decomposed into both vertical and horizontal vector components) can be quantified using GISAXS, which probes both components. To demonstrate that adding IL brings specific advantage to the kinetics of ordering in achieving parallel ordering, we start with the intermediate M_w of 33k−33k for the PS−PMMA system. When heated for a sufficient time (>18 h at 170 °C), we find that these can achieve an essentially perfect parallel orientation without added IL (up to $6L_o$). However, to demonstrate a kinetic advantage of ordering BCP films with IL in this case, we annealed them for a shorter time window. We initially chose an intermediate film thickness of h = 230 nm [$\approx 6-7L_o$] and thermally annealed the films at 170 °C for 9 h. This duration of time and temperature of annealing are not sufficient to induce complete parallel lamellar ordering in this system without IL.

While it is known that island and hole evolution occurs through fractional increments of domain spacing, L_o,[20,21,42,45] here we also validate the hypothesis that this temporal structure evolution of islands and holes in films of incommensurate thickness is indicative of the degree of partial to complete layer stratification within the lamellar BCP films. An essential result is that when the islands and holes reach one domain height/depth (L_o) on the BCP surface, there is complete parallel stratification within the BCP film. This temporal correlation of surface domain structure height evolution to internal BCP film stratification is borne out by AFM and GISAXS confirmation of progressive disappearance of perpendicular meandering lamellae in the films. This correlation can therefore be used to detect lamellae stratification in thicker films. The presence of IL in the BCP film accelerates the kinetics of the process and enhances the range of surface-directed BCP-layer stratification from substrate and air interfaces.

The AFM profile is shown for thermally annealed PS−PMMA 66k films for the h = 230 nm incommensurate thickness films, with and without IL (Figure 1). Without IL, when the neat BCP is heated at 170 °C for 9 h, the time is insufficient to achieve complete parallel ordering for this M_w BCP. Figure 1A shows that when there is no IL additive, the surface of the film is flat, i.e., no islands and holes are formed on the surface. Although it can be reasoned that a commensurate condition may be present that suppresses the formation of the islands and holes, this is less likely as h is about 230 nm with about 37 nm domain length for these polymers, corresponding to 6.2 domain lengths, i.e., ($h \neq n + (1/2)L_o$). Thus, the only way the development of frustration can be released in these films is through the formation of islands and holes, and we also directly confirm this in the limit of long-time annealing (18 h at 170 °C). As in previous studies, the evolution of islands and holes proceeds in fractions of the stable one domain length (L_o), i.e., the surface height increases from surface roughness to a quarter to one-half and finally to a stable single-domain-length structure.[20,21,42,45] As the percentage of IL in these films is increased to 5 mass (fraction) % relative to the BCP, the surface height profile starts to progressively oscillate (Figure 1B). When IL is

https://doi.org/10.1021/acs.macromol.0c02546
Macromolecules 2021, 54, 4531−4545

incrementally added to the BCP, the kinetics of internal BCP layered ordering improves rapidly and well-defined levels of island and hole formation are observed at the film surface (Figure 1C−F).

From Figure 1, it can be seen that for ILs of 10 mass % (Figure 1C) and 15 mass % relative concentration (Figure 1D), the BCP film surface shows well-formed islands and holes of height L_o (≈37 nm), showing that they have incommensurate thickness.[45,51] Thus, neat (no IL) melt-annealed BCP domain spacings (≈37 nm) are achieved, even in these relatively high-IL-fraction-containing films. This is consistent with the fact that the IL is ultimately mostly removed from the BCP film during the vacuum annealing process (see Figures S3 and S4),[28] but not before it plays a significant role in accelerating the layered ordering in the BCP films. As the IL content is increased to 20% relative mass or higher, simultaneous presence of islands and holes is observed. Our investigation shows that heating the same film longer can alter the surface height profile further in a hierarchy of multiples of island and holes and may have many configurations, such as islands on top of islands or holes within holes. This interesting observation is also sometimes made in block copolymer films and one that we believe has its origin in sluggish in-plane versus out-of-plane mobility. Subsequently, the holes can lead to dewetting, which we believe is of an autophobic dewetting nature. It can also be seen that at very high IL content (40 relative mass % or higher) the structure of the BCP film clearly enhances formation of only holes at the film surface, however with a rough surface formation, thus reflecting a high degree of stratification through the film interior. The average depths of the island and hole are plotted in Figure 1G, which shows the enhancement of surface evolution to a stable structure. For these BCP films annealed in a limited time, 10 mass % IL and higher was required to give the full domain height of L_o of island and holes, although at IL greater than 20 mass %, the quality of the surface features starts to deteriorate in the presence of multiple-domain-length features.

Next, we examine correlations between surface island and hole heights by AFM in Figure 1 and the corresponding GISAXS in Figure 2. The trend in Figures 1 and 2 reveals that as the surface features attain heights corresponding to L_o, the domain thickness of the island and hole structure at the film surface and the in-plane meandering within the film disappear. Specifically, in GISAXS in Figure 2, it is apparent that at 10 mass % IL by relative mass, the in-plane peak completely disappears, which indicates no out-of-plane lamellae, which exactly corresponds to the AFM image in Figure 1C in which islands and holes of full height L_o appear at the surface. This validates that island and hole formation of height L_o in films occurs only in L-BCP films with a completely parallel layering state of lamellae within them. From Figure 2, the peak in q_y for no IL additive corresponds to 0.17 Å^{-1}, and using $L = \frac{2\pi}{q_y}$, the domain length is 37 nm, which is in perfect coherence with the theoretical domain length obtained using SSL, $L = \frac{4}{\sqrt{6}}\left(\left(\frac{3}{\pi^2}\right)^{1/3}\right) bN^{2/3}\chi^{1/6}$,[9] where b is a segmental size parameter, and this quantity is estimated to be on the order of 0.7−0.85 (b = 0.85 assumed in this calculation); χ for PS−PMMA[18] is approximated by the usual phenomenological relation $\chi = A - \frac{B}{T}$, where the "entropic contribution" to χ is A = 0.028 and the enthalpic contribution is B = 1.9. As the IL increases, the in-plane peak disappears and the surface island and holes of one-domain-length form, which is a manifestation of the complete parallel ordering attained through use of the IL. Further addition of IL beyond 10% IL leads to a low-q upturn in GISAXS, suggesting weak long-wavelength scale fluctuations in the in-plane structure of the film caused by excess IL beyond what is needed for stratification. We think this happens due to the small-scale structure disruption in the polymer during the evaporation of the IL when annealed. Therefore, 0−15% IL may be considered the optimal range, sufficient to induce rapid ordering in this 66k M_w PS−PMMA system without causing structure disruption. As such, there is an optimal balance between IL-concentration-enabled ordering properties and their removal rate. This is because the ability of the PMMA fraction to sequester the IL without losing BCP lamellar ordering properties is limited, not infinite. Too high a IL content likely causes structure disruption as not enough of it evaporates within the long-term annealing window, leading to long-range correlated disordered or multigrain ordered mosaic structures giving rise to a low-q GISAXS peak. Hence, there is an upper IL limit. On the lower limit side, our observation shows that a small, but equilibrium amount of IL remains behind in the sample even after annealing, as also confirmed in Figure S4. As long as the amount of IL used is in the vicinity of a balance window of a quasi-equilibrium amount, and the amount of IL used is not too high to cause structure disruption despite significant evaporation, it may be considered an optimal range. We have found that to be between 0 and 15% mass fraction IL relative to the polymer.

We next examine IL-induced ordering in films of the same intermediate M_w system but with much thicker dimensions, from h ≈ 700 to 750 nm, which are on the order of up to 20 times the domain length, L_o. For a lower M_w lamellar system, i.e., dPS−PMMA 19.5k−18k, it was shown earlier by Samant et al.[3] that the evolution of complete parallel ordering by soft shear is realizable up to a micrometer in thickness, and they were found to be useful in capacitor applications since they display a high breakdown strength.[3] Xu et al. worked with similar M_w films (70.5k) as used in this work (66k) and showed that thick films on the order of 400−800 nm, even after annealing for an extended period of time, retain the in-plane meandering, and even after surface engineering to increase the surface driving force, the film did not attain complete parallel ordering.[16] They showed that parallel lamella even with a highly selective surface does not extend beyond five domain lengths, whereas for a less selective surface, the lamella extends to only three domain lengths. These findings show that aligning parallel lamellae beyond five domain lengths on a bare silicon surface even with creating a high surface driving force is an arduous task for such low χ BCPs. Therefore, we hypothesize that such an alignment is possible without having a higher interfacial driving force using IL to enhance χ, the block segregation parameter, and the mobility of the segments by transiently reducing the T_g during the ordering process. Enhanced mobility of the segment and higher χ were found to help in the propagation of parallel lamellar stratification and obtain surface-directed correlation length as high as 20 times the domain length L_o.

As we have shown earlier, a signature of the presence of mostly in-plane meandering lamellae in thermally annealed neat L-BCP films is the lack of (L_o high) stable islands and holes. Therefore, with 66k M_w symmetric PS−PMMA, in films of thickness beyond 3−6L_o, without surface engineering, the

https://doi.org/10.1021/acs.macromol.0c02546
Macromolecules 2021, 54, 4531−4545

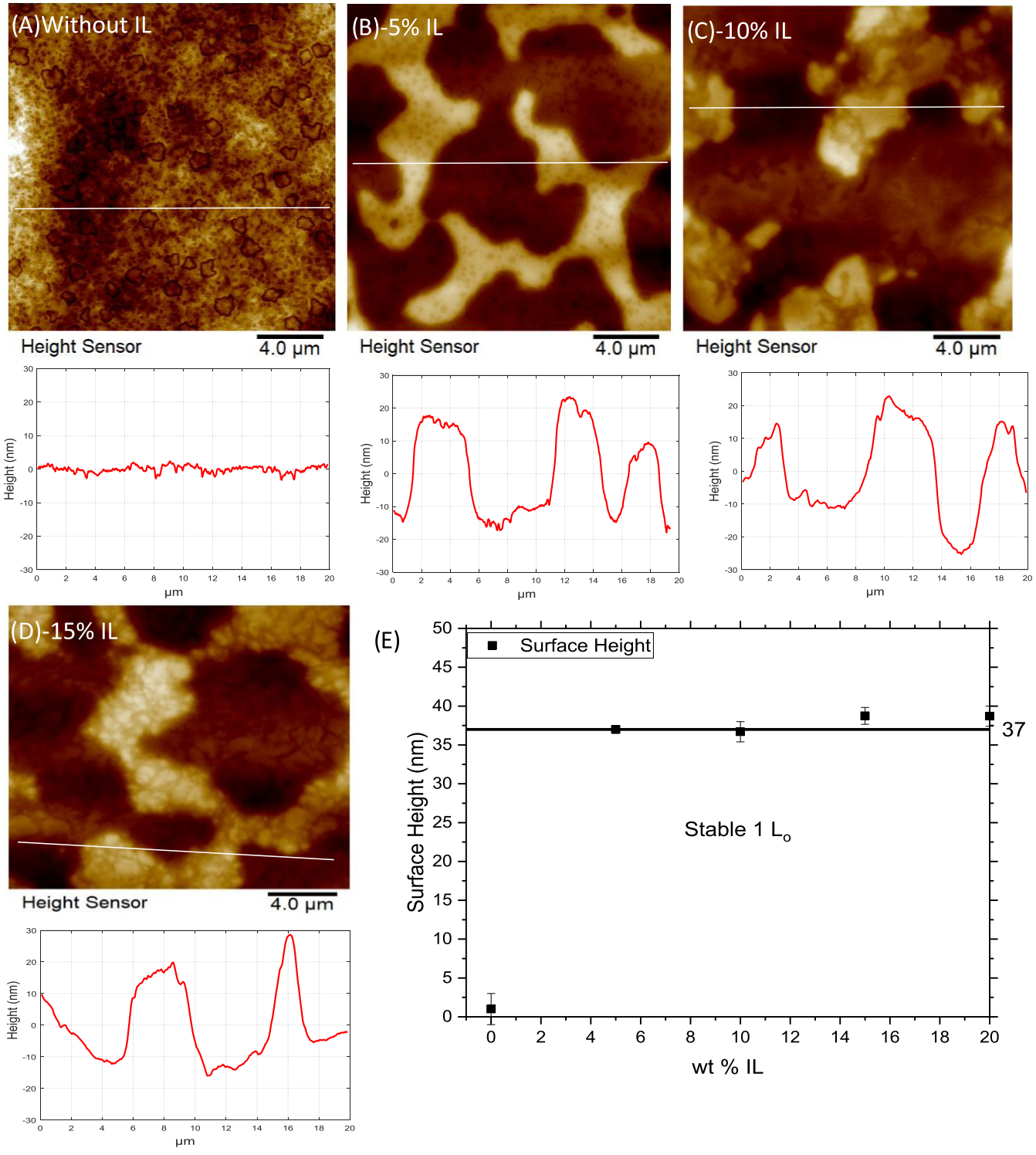

Figure 3. AFM morphology and line-cuts of the PS-*b*-PMMA 33k−33k ordered using thermal annealing (TA) at 185 °C for 40 h for thickness *h* of about 700−750 nm. (A−D) With different fractions of IL. (E) Evolution of morphology on the surface of lamellar systems as the amount of IL increases. The island and hole structures appear at 5% relative mass fraction of IL. The uncertainty measurements were taken from the standard deviation from average values obtained from the AFM line-cut profile.

formation of in-plane meandering is almost inevitable in melt-annealed films with no IL even with extensive annealing times. Consistent with these ideas and observation, Figure 3a shows that when these thick (≈700−750 nm) films were heated at 185 °C for 40 h, the films without IL did not form any islands and holes. However, if IL is added even at 5% by relative mass to the PS−PMMA block copolymer in the film casting solution, we observed that islands and holes formed, with the surface feature height reaching the stable one-domain-length height, indicative of complete internal parallel stratification within the film.[20,45,52]

At higher IL mass % (>10% IL mass %), the surface retains the island and hole structure, but cracks appear on the surface, suggestive of annealing past the required time for ordering, due

https://doi.org/10.1021/acs.macromol.0c02546
Macromolecules 2021, 54, 4531−4545

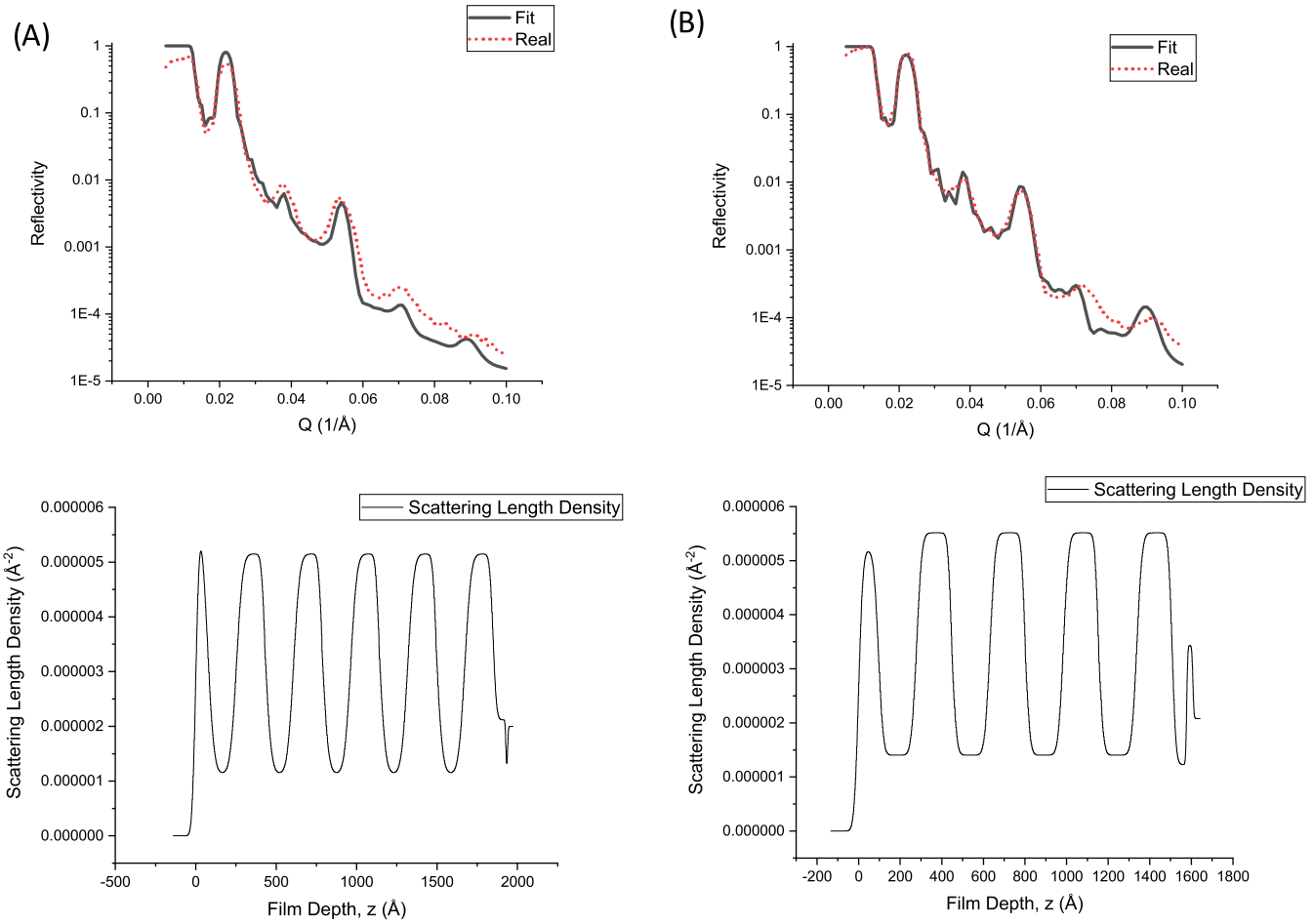

Figure 4. NR profile of annealed dPS−PMMA 29.5k−32.5k (A) without IL and (B) with 10% IL, and the bottom figures are the respective SLD profiles.

to the film's inability to accommodate the large variations in stresses caused by the film's undulation. Our hypothesis is that since IL induces faster ordering of predominantly the PMMA block, heating too long may lead to structure breakage due to equilibration stresses with in the glassy PS film, causing an undulating film height, which sometimes also causes dewetting of the films during long annealing. In general, however, we conclude that an appropriate amount of IL can induce defect-free ordering in thicker films of this intermediate M_w PS−PMMA L-BCP regime, which was not achievable without IL. We next investigate the intermediate M_w films (dPS−PMMA 29.5k−32.5k) through neutron reflectivity (NR) of modest 200 nm thick films, ordered using thermal annealing for 8 h at 170 °C. The data fit for the system, by comparing the scattering length density (SLD) profiles in Figure 4A,B, suggests that the scattering length density (SLD) profile enhanced from a sinusoidal z-composition variation of dPS and PMMA alternating domains to a more rectangular uniform lamellar organization, responsible for sharper interfaces when 10% IL is added to the system. Moreover, fitting reveals that the PS-b-PMMA junction interfacial width without IL is 58 ± 1 Å, and with IL, it reduces to 40 ± 2 Å. This is sharper than the previously reported values of ≈50 Å.[52,53] It can be conveniently shown using the Helfand approximation,[54] $w = \frac{2a}{\sqrt{6\chi}}$, that the χ increases by a factor of ≈2 times from the value of about 0.04−0.084. This is in line with the previously reported enhancement of χ with IL reported using techniques such as small-angle X-ray scattering (SAXS).[28,55] Such enhancements validate our earlier hypothesis of the enhancement of χN to be the driving force for the enhanced lamellar orientation in thicker films of higher M_w.

High-Molecular-Mass PS−PMMA (65k−62.5k, M_w = 127.5k). We next extend our focus to a higher M_w lamellar system that is even more difficult to order using thermal annealing in the neat melt state. Earlier, it was shown that thermal annealing of PS−PMMA of high M_w (100k) forms terraced structures with dislocations present in the terraces.[20] Some other earlier studies by Coulon et al. and Russell et al. on relatively higher M_w lamellar (≈100k) systems were performed on either block being deuterated, while cast on preferential surfaces through different substrate pretreatment, or coating such as gold or carbon, and spin coated from slow evaporating solvents and annealed for longer time. The film's internal structures were studied by ToF-SIMS only, but no specific study was performed for in-plane meandering of lamellae.[38,39] ToF-SIMS reveals the sinusoidal order from the surface with decaying intensity as the film depth increases.

For this high-M_w-range L-BCP study, we used PS−PMMA of the total M_w of 127.5k (65k−62.5k) to cast films in the thickness range h ≈ 300−400 nm by flow-coating on UV-treated silicon substrates and thermal annealing at 185° for 40 h. The AFM surface profile in Figure 5, of IL-containing films that were thermal-annealed for 40 h at 185 °C, shows that the

https://doi.org/10.1021/acs.macromol.0c02546
Macromolecules 2021, 54, 4531−4545

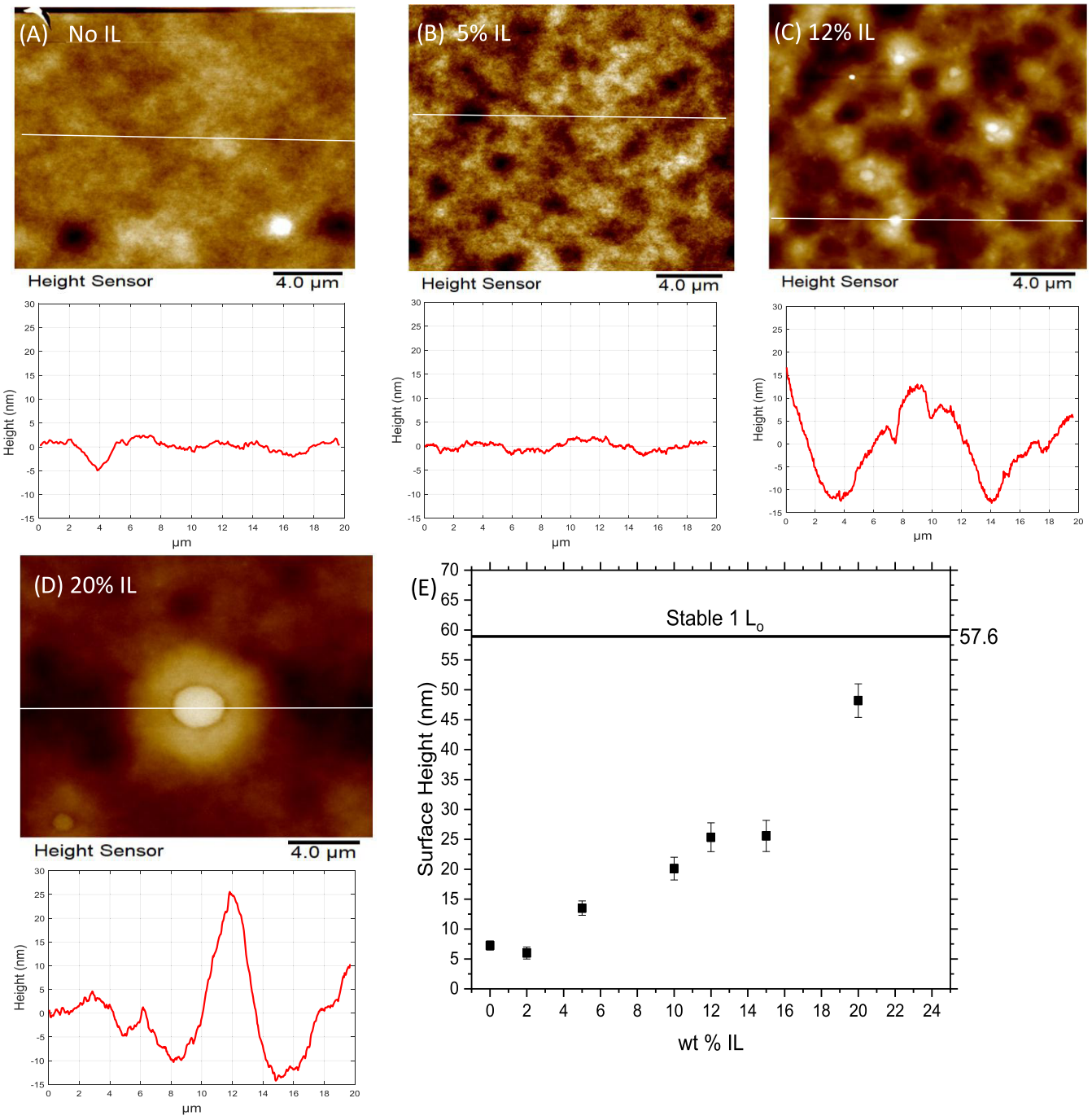

Figure 5. AFM morphology images of the PS-*b*-PMMA 65k−62.5k ordered using TA at 185 °C for 40 h for a thickness of about 350−400 nm (A−D). The evolution of morphology on the surface for lamellar systems from the AFM surface profile as the amount of IL increases can be seen. Even with insufficient TA, the in-plane meandering almost completely disappears at 20% IL by mass, although the surface may still not have completely attained a thickness of L_o. The uncertainty measurements were taken from the standard deviation from average of estimates taken from the AFM line-cut profile.

surface height profile increases steadily from surface roughness to an almost complete single-domain-high island and hole structure, which is still not as well-developed on the surface. However, annealing longer and/or at higher temperatures could make the surface structure more well-formed. Using the SSL approximation as earlier, the theoretical domain length is 57.6 nm. Thus, in the presence of no additives, assuming this domain length in 350 nm films, six domains should be present through the film. Ordering neat L-BCP films of such thickness and M_w combination is an elusive task, as can be seen in the AFM of Figure 5.

The enhancement in the ordering of this high M_w film in the presence of IL is ascertained from the in-plane GISAXS line-cut profile seen in Figure 6, which shows that the in-plane structure completely disappears when the IL mass content in the films increases to 20%, and the same is true of the AFM surface images when the surface height increases to the order of 1 domain spacing.

https://doi.org/10.1021/acs.macromol.0c02546
Macromolecules 2021, 54, 4531−4545

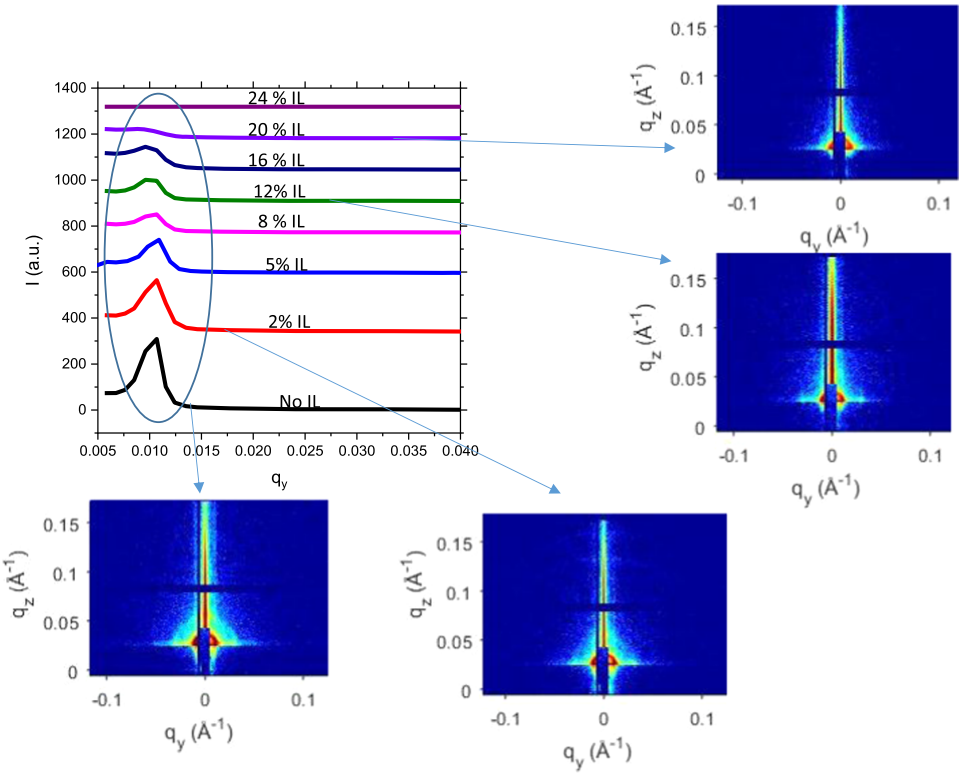

Figure 6. GISAXS line-cut profile obtained from taking the cumulative q_y along all q_z. In-plane meandering is revealed below 16% IL and disappears above that.

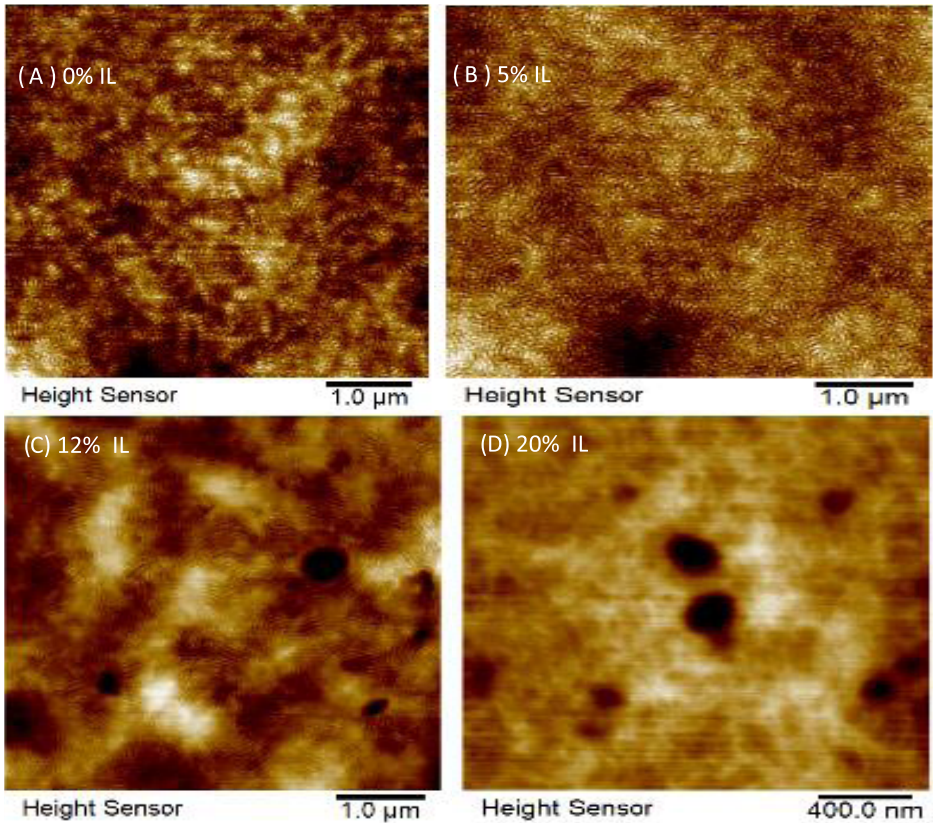

Figure 7. AFM morphology of laser-ablated films of PS-*b*-PMMA 65k−62.5k ordered using TA at 185 °C for 40 h for thickness of about 350−400 nm (A−D). The films were etched about 140−150 nm using UV radiation of wavelength 193 nm for 30 min. The ablated AFM profile shows that as IL increases the in-plane meandering disappears and a parallel orientation with island and hole structures is assumed.

https://doi.org/10.1021/acs.macromol.0c02546
Macromolecules 2021, 54, 4531−4545

From Figure 6, the in-plane GISAXS line-cut profile shows a peak at 0.107 A^{-1} in q_y, arising from the meandering of vertical lamellae in the middle of the film. This corresponds to a domain length of about 58.7 nm. Using SSL, the domain length for this polymer is 57.6 nm.[9] The peak at 0.107 A^{-1} does not vary much as the percentage of IL increases; thus, it can be concluded that the in-plane meandering structure varies little with added IL. However, from Figure 8, the ToF-SIMS image of the same BCP system, it is seen that the out-of-plane domain structure varies significantly even when a very low mass fraction of IL is added. This can be explained using the assumption that IL-induced swelling is only accommodated in the out-of-plane direction by chain rearrangements.

To investigate the presence of the in-plane meandering in the middle of the films, we performed UV ablation to the films to remove about 150 nm of the films in 45 min using a 193 nm UV wavelength (etch rate of 3.33 nm/min). When etched from the film surface top-down by UV, the etching process is apparently uniform and therefore the etched surface at any depth is almost conformal to the original surface topography of islands (or holes). The hole structure may etch at a slightly lower rate than the island structure since more UV rays can etch the top surface. Also, PS and PMMA have slightly different etch rates, but given a lamellar geometry, this differential rate would mean slower etch through the parallel PS or the PMMA layer, but the topography would still be preserved. The AFM profile of the image in the UV-etched region can be seen in Figure 7, showing the presence of meandering vertical domains in films with no IL.

The domain length of these in-plane structures in Figure 7 is about 57 nm, taken from the average section profile from AFM. As IL increases, the in-plane meandering reduces, and islands and holes start to appear (at 12 mass % IL) throughout the film with meanderings around them. It was shown earlier that in-plane meandering usually surrounds the islands and holes, forming a terraced structure.[20,21] Through repetitive measurements from the AFM profile, as IL is increased to 0−8 mass % in the film, the domain size of the in-plane meandering stays roughly the same at about 57 nm. At higher IL concentrations, of 12% or higher, the in-plane domain structure increases by a few nanometers only, for example, at 12%, it is 62 nm and stays almost constant through that value until the meandering completely disappears at 20% IL. Notice that this slight in-plane swelling occurs only when the meandering has mostly disappeared, and more in-plane space is made available by polymers rearranging in the out-of-plane structure. In our recent unpublished work, we have shown that in-plane restructuring is more difficult to achieve than out-of-plane restructuring due to the film pinning effect.

Figure 8 shows the ToF-SIMS for the same high-M_w films heated at 230 °C for 24 h. In the graph, the red line is the silicon signal and is well-developed only at the end, an indication that the films are well-developed without any dewetting. The green line is the IL, absent in neat films, and appears as a sinusoidal peak in IL-containing films showing that IL has migrated to the PMMA phase as it follows the alternating domain pattern of the PMMA layers.

The black curve is the PS signal, and it is strong compared to the blue PMMA peak. We posit this to be due to the positive ToF-SIMS analysis measured here being more sensitive to the generation of the $C_7H_7^+$ (from PS) fragments than the $C_4H_5O^+$ (from PMMA) fragments as the data has a much higher relative intensity. Figure S4 shows the negative ToF-SIMS analysis of the PMMA homopolymer (of 30k M_w) before and after annealing containing 50% IL, and it is more sensitive to the IL or PMMA detection. The integrated profile taken under the graph shows that about 99% IL is lost after annealing at 180 °C for 24 h. We believe that the remnant 1% IL are molecules in direct contact with PMMA chains that are more strongly bound, but further studies are needed to verify this. The removal of almost 99% IL from PMMA is the reason we do not observe non-lamellar morphologies due to swelling as seen in the literature involving additives, such as homopolymers and polymer-grafted nanoparticles (PGNPs) to the BCP system, even when up to 40 wt % IL is added to the BCP. However, unlike other additives described that reside in the film even after annealing, our findings and earlier literature suggest that the IL leaves upon annealing at elevated temperatures at low vacuum pressures, preserving the intrinsic BCP morphology.

Without the IL, no island and hole are formed even at interfaces, as seen in Figure 8A with the ToF-SIMS and optical

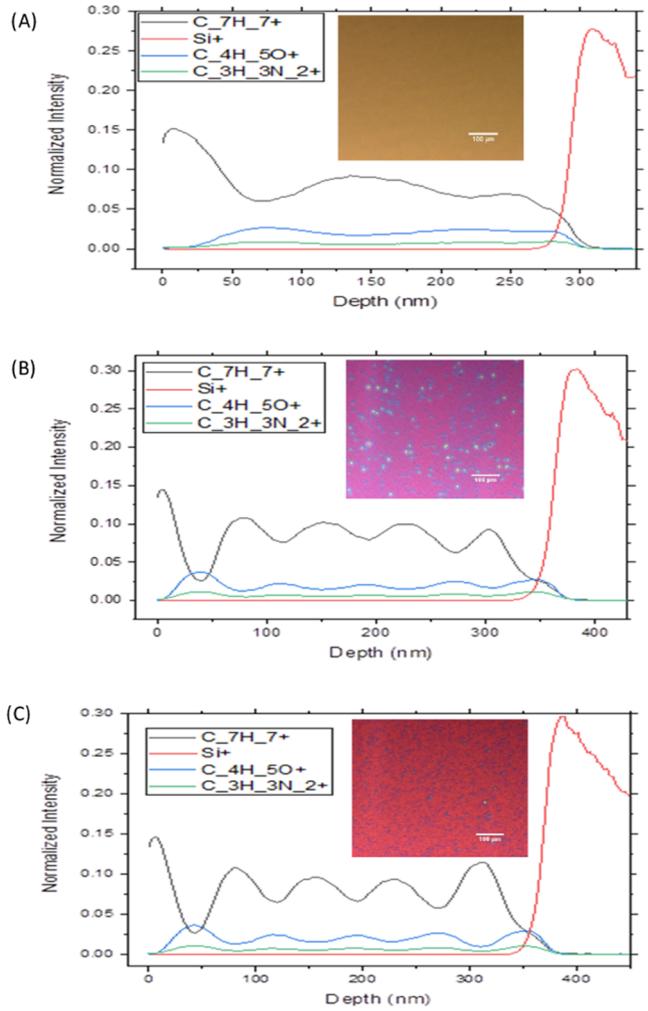

Figure 8. ToF-SIMS profile of 350−400 nm PS-*b*-PMMA films of M_w 65k−62.5k heated at 240 °C for 24 h. It can be seen from ToF-SIMS and the inset optical microscopy image in this high-M_w and high-thickness regime that (A) without IL there is apparently no order or even any island and hole structures in optical microscopy images. With IL (B) 5% relative mass and (C) 10% relative mass, the sample developed sinusoidal ordering and the island and hole structures. Scale bar represents 100 μm.

https://doi.org/10.1021/acs.macromol.0c02546
Macromolecules 2021, 54, 4531−4545

microscopy. However, even with 5% (Figure 8B) IL, a sinusoidal pattern develops, and the optical microscope image shows the presence of islands and holes. The pattern from the 10% IL relative to the polymer is slightly more developed than the 5% IL, with islands and holes seen from optical images. Since well-formed islands and holes in this high-M_w system are larger in size, AFM analysis was not utilized. The profile in the IL-containing ordered film shows, as summarized in Table 1, that the interface layers are on the order of half the domain length, and the lamellar middle layers are on the order of 76 nm, which is significantly higher than the 57.6 nm, theoretically predicted for this polymer system. If we assume $L_o \sim \chi^{1/6}$, and the change in χ is the sole contributor to the change in domain length, then χ has to increase by 5.43 times to accommodate this change, which is unusually large. Notably, this assumption may not be valid since it does not take the IL swelling (remnant IL or vitrified swollen structure) effect into account, and as such the NR result based on interfacial width narrowing is more reliable for accounting for the enhancement of χ. Moreover, we also notice that the swollen domain length at different ILs (5 or 10 mass %) stays almost constant (at 76 nm). This may be due to the evaporation of excess IL, while retaining an amount that uniformly wets the PMMA-rich interfacial layer. The loss of IL was noticed earlier by Chen et al.;[28] however, excess IL has a higher ordering effect as revealed in this paper because IL and PMMA are miscible over a larger compositional range[25] and the T_g of the polymer decreases steadily as more IL is added. Thus, higher mobility induces faster ordering before excess IL is evaporated.

Table 1. Length of the First PS Layer, the Middle PS−PMMA Domain Alternating Layers, and the PMMA Layer near the Substrate Surface[a]

% IL	air interface layer (nm)	average domain length (nm)	wafer interface layer (nm)
0	69.22	not quantifiable	23.59
5	39.51	76.28 ± 2.73	39.84
10	43.87	76.33 ± 3.83	38.84

[a]The uncertainty estimates are defined by the standard deviation of the average values of the peak-to-peak distance or trough-to-trough distances.

The loss of IL when heated in a vacuum environment above 140 °C is also apparent in Figure S3 in homopolymer PMMA (not PS−PMMA) and IL films. It can be seen that the film thickness, in PMMA with 50% IL (by weight) films, decreases by up to 30% (from 200 to 140 nm, i.e., volumetrically) when heated for an hour. Furthermore, negative ToF-SIMS analysis for IL by its chemical composition in the film shows that after annealing at 180 °C for 24 h in a vacuum condition, the film height decreases by 30% or about 99% IL is lost. Earlier reports of mass loss[28] and our observation of thickness loss demonstrate that IL-containing films lose the IL through evaporation under vacuum annealing conditions. We believe that although this would not occur at room pressure, the vacuum substantially lowers the boiling point of the IL, so that it vaporizes at the high annealing temperature and longtimes. Thermal annealing of even higher M_w of PS−PMMA of 80k−80k for 2 days at 240 °C did not reveal any ordering in non-IL or IL-containing films (Figure S1). Also, a scaling relation derived from three low-to-high M_w lamellar systems using NR shows that the scaling constant for domain length as the number of segment changes is almost the same for both IL- and non-IL-containing films (Figure S2). This suggests that the effect of IL on different M_w systems show a similar enhancement of χ, affecting predominantly the interfacial width rather than the domain spacing, along with enhanced rate of ordering generally.

Thus, we conclude that increases in the PS−PMMA χ parameter, without a significant change in the strong wetting of the silicon oxide surface by the PMMA domain, are responsible for the enhanced orientational order in the symmetric PS−PMMA systems to induce through-thickness parallel lamellar ordering for higher-M_w and higher-thickness films. In addition, the enhanced mobility and diffusivity of the blend system are due to the lowered T_g as determined in the literature, which has a significant contribution to this enhanced z-stratification of the lamellae effect. Further, the effect of any change in the surface energy and interfacial surface tension, since IL has a lower surface energy, may also be a contributing force, but such changes are not quantified in the present work. Use of IL to surmount parallel orientational controlled ordering in high-molecular-weight and high-thickness films can open avenues to their applications of lamellar block copolymer films in areas previously unattainable.

CONCLUSIONS

We have demonstrated that adding IL to higher-molecular-mass and higher-film-thickness PS−PMMA lamellar block copolymer films has unique advantages in enhancing the orientational order of lamellae parallel to the substrate and achieving ordering in BCP systems that are kinetically limited under thermal annealing conditions only. In particular, we have significantly improved the kinetics of ordering in such kinetically frustrated films and have also demonstrated the formation of through-thickness complete parallel ordering with a classic rectangular composition of pure block domains in symmetric PS−PMMA films. The careful increment of IL addition on orientational ordering was tracked by the AFM approach to one domain size of the island and hole structure that exists at the film surface, which remained constant thereafter with increased IL addition. This evolution of the surface structure was correlated to the development of the film's internal layer and interface profile by ToF-SIMS, GISAXS, and NR data fitting. Further, the in-plane meandering completely disappears in these higher-molecular-mass and higher-thickness lamellar films. Specifically, we have demonstrated that IL enables ordering in the high-molecular-mass (>100k) regime, where complete parallel ordering without any meandering is difficult to achieve for low-χ block copolymers. We attribute this to an enhanced χ and segmental mobility coupled with surface tension differential between blocks to enable this enhanced stratification. Finally, we have shown how IL allows low-χ polymers to attain high-χ polymer characteristics without getting arrested in a metastable state, inducing long-range ordering, while almost completely self-removing themselves from the structure. These findings are important as they can enable the application of these films in several emerging energy storage systems, flow cells, capacitors, and barrier materials as parallel efforts to order BCPs on flexible substrates are emerging.[9,56]

https://doi.org/10.1021/acs.macromol.0c02546
Macromolecules 2021, 54, 4531−4545

■ ASSOCIATED CONTENT

Supporting Information

The Supporting Information is available free of charge at https://pubs.acs.org/doi/10.1021/acs.macromol.0c02546.

Additional data on ToF-SIMS (Figure S1) investigating the depth profile of PS−PMMA BCP of 80k−80k M_w with and without IL; NR profiles of three different symmetric dPS−PMMA BCP systems and the scaling relationship derived from them with and without IL (Figure S2); decrease in film height as homopolymer films containing IL and no IL are heated at different annealing conditions for different times under a vacuum condition (Figure S3); negative ToF-SIMS depth profile of a homopolymer PMMA film containing IL before and after annealing (Figure S4); and TGA of the EMIM TFSI (Figure S5) (PDF)

■ AUTHOR INFORMATION

Corresponding Authors

Jack F. Douglas − *Materials Engineering Laboratory, National Institute of Standards and Technology, Gaithersburg, Maryland 20899-3460, United States;* orcid.org/0000-0001-7290-2300; Email: jack.douglas@nist.gov

Alamgir Karim − *Department of Chemical and Biomolecular Engineering, University of Houston, Houston, Texas 77204-4004, United States;* orcid.org/0000-0003-1302-9374; Email: akarim3@Central.UH.EDU

Authors

Ali Masud − *Department of Chemical and Biomolecular Engineering, University of Houston, Houston, Texas 77204-4004, United States*

Melanie Longanecker − *Department of Polymer Engineering, The University of Akron, Akron, Ohio 44325, United States*

Sonal Bhadauriya − *The University of Akron, Akron, Ohio 44325, United States*

Maninderjeet Singh − *Department of Chemical and Biomolecular Engineering, University of Houston, Houston, Texas 77204-4004, United States*

Wenjie Wu − *Department of Chemical and Biomolecular Engineering, University of Houston, Houston, Texas 77204-4004, United States*

Kshitij Sharma − *Department of Chemical and Biomolecular Engineering, University of Houston, Houston, Texas 77204-4004, United States*

Tanguy Terlier − *SIMS Laboratory, Shared Equipment Authority, Rice University, Houston, Texas 77005-1892, United States;* orcid.org/0000-0002-4092-0771

Abdullah M. Al-Enizi − *Department of Chemistry, College of Science, King Saud University, Riyadh 11451, Saudi Arabia;* orcid.org/0000-0002-3967-5553

Sushil Satija − *Center for Neutron Research, National Institute of Standards and Technology, Gaithersburg, Maryland 20899-3460, United States*

Complete contact information is available at: https://pubs.acs.org/10.1021/acs.macromol.0c02546

Notes

Certain commercial materials and equipment are identified to specify adequately the experimental procedure. In no case does such identification imply recommendation by the National Institute of Standards and Technology, nor does it imply that the material or equipment identified is necessarily the best available for this purpose.

The authors declare no competing financial interest.

■ ACKNOWLEDGMENTS

A.K. would like to acknowledge the funding support by the National Science Foundation (NSF) via Grant DMR-1905996. A.K. and A.M.A.-E. also extend their sincere appreciation to Researchers Supporting Project number (RSP-2021/55), King Saud University, Riyadh, Saudi Arabia, for funding related to the research. This research used resources of the Advanced Photon Source, a U.S. Department of Energy (DOE) Office of Science User Facility, operated for the DOE Office of Science by Argonne National Laboratory under Contract no. DE-AC02-06CH11357. ToF-SIMS analyses were carried out with support provided by the National Science Foundation CBET-1626418. We acknowledge Guangcui Yuan at the NIST Center for Neutron Research and the neutron reflection beam time made available for this study. This work was conducted in part using resources of the Shared Equipment Authority at Rice University.

■ REFERENCES

(1) Sinturel, C.; Bates, F. S.; Hillmyer, M. A. High χ-Low N Block Polymers: How Far Can We Go? *ACS Macro Lett.* **2015**, *4*, 1044−1050.

(2) Lin, Y. H.; Yager, K. G.; Stewart, B.; Verduzco, R. Lamellar and Liquid Crystal Ordering in Solvent-Annealed All-Conjugated Block Copolymers. *Soft Matter* **2014**, *10*, 3817−3825.

(3) Samant, S. P.; Grabowski, C. A.; Kisslinger, K.; Yager, K. G.; Yuan, G.; Satija, S. K.; Durstock, M. F.; Raghavan, D.; Karim, A. Directed Self-Assembly of Block Copolymers for High Breakdown Strength Polymer Film Capacitors. *ACS Appl. Mater. Interfaces* **2016**, *8*, 7966−7976.

(4) Gartner, T. E.; Morris, M. A.; Shelton, C. K.; Dura, J. A.; Epps, T. H. Quantifying Lithium Salt and Polymer Density Distributions in Nanostructured Ion-Conducting Block Polymers. *Macromolecules* **2018**, *51*, 1917−1926.

(5) Samant, S.; Strzalka, J.; Yager, K. G.; Kisslinger, K.; Grolman, D.; Basutkar, M.; Salunke, N.; Singh, G.; Berry, B.; Karim, A. Ordering Pathway of Block Copolymers under Dynamic Thermal Gradients Studied by in Situ GISAXS. *Macromolecules* **2016**, *49*, 8633−8642.

(6) Phillip, W. A.; O'neill, B.; Rodwogin, M.; Hillmyer, M. A.; Cussler, E. L. Self-Assembled Block Copolymer Thin Films as Water Filtration Membranes. *ACS Appl. Mater. Interfaces* **2010**, *2*, 847−853.

(7) Mansky, P.; haikin, P.; Thomas, E. L. Monolayer Films of Diblock Copolymer Microdomains for Nanolithographic Applications. *J. Mater. Sci.* **1995**, *30*, 1987−1992.

(8) Black, C. T.; Ruiz, R.; Breyta, G.; Cheng, J. Y.; Colburn, M. E.; Guarini, K. W.; Kim, H.-C.; Zhang, Y. Polymer Self Assembly in Semiconductor Microelectronics. *IBM J. Res. Dev.* **2007**, *51*, 605−633.

(9) Bates, F. S.; Fredrickson, G. H. Block Copolymer Thermodynamics: Theory and Experiment. *Annu. Rev. Phys. Chem.* **1990**, *41*, 525−557.

(10) Yager, K. G.; Forrey, C.; Singh, G.; Satija, S. K.; Page, K. A.; Patton, D. L.; Douglas, J. F.; Jones, R. L.; Karim, A. Thermally-Induced Transition of Lamellae Orientation in Block-Copolymer Films on "neutral" Nanoparticle-Coated Substrates. *Soft Matter* **2015**, *11*, 5154−5167.

(11) Bita, I.; Yang, J. K. W.; Jung, Y. S.; Ross, C. A.; Thomas, E. L.; Berggren, K. K. Graphoepitaxy of Self-Assembled Block. *Science* **2008**, *321*, 939−943.

(12) Mansky, P.; Liu, Y.; Huang, E.; Russell, T. P.; Hawker, C. Controlling Polymer-Surface Interactions with Random Copolymer Brushes. *Science* **1997**, *275*, 1458−1460.

(13) Singh, G.; Yager, K. G.; Berry, B.; Kim, H.; Karim, A. Dynamic Thermal Field-Induced Gradient Soft-Shear for Highly Oriented Block Copolymer Thin Films. *ACS Nano* **2012**, *6*, 10335−10342.
(14) Modi, A.; Bhaway, S. M.; Vogt, B. D.; Douglas, J. F.; Al-enizi, A.; Elzatahry, A.; Sharma, A.; Karim, A. Direct Immersion Annealing of Thin Block Copolymer Films. *ACS Appl. Mater. Interfaces* **2015**, *7*, 21639−21645.
(15) Xu, T.; Zhu, Y.; Gido, S. P.; Russell, T. P. Electric Field Alignment of Symmetric Diblock Copolymer Thin Films. *Macromolecules* **2004**, *37*, 2625−2629.
(16) Xu, T.; Hawker, C. J.; Russell, T. P. Interfacial Interaction Dependence of Microdomain Orientation in Diblock Copolymer Thin Films. *Macromolecules* **2005**, *38*, 2802−2805.
(17) Kim, Y.; Yong, D.; Lee, W.; Jo, S.; Ahn, H.; Kim, J. U.; Ryu, D. Y. Preferential Wetting Effects on Order-to-Disorder Transition in Polystyrene-b-Poly(2-Vinylpyridine) Films: A Reconsideration on Thickness Dependence. *Macromolecules* **2018**, *51*, 8550−8560.
(18) Russell, T. P.; Hjelm, R. P.; Seeger, P. A. Temperature Dependence of the Interaction Parameter of Polystyrene and Poly (Methyl Methacrylate). *Macromolecules* **1990**, *23*, 890−893.
(19) Maher, M. J.; Rettner, C. T.; Bates, C. M.; Blachut, G.; Carlson, M. C.; Durand, W. J.; Ellison, C. J.; Sanders, D. P.; Cheng, J. Y.; Willson, C. G. Directed Self-Assembly of Silicon-Containing Block Copolymer Thin Films. *ACS Appl. Mater. Interfaces* **2015**, *7*, 3323−3328.
(20) Carvalho, B. L.; Thomas, E. L. Morphology of Steps in Terraced Block-Copolymer Films. *Phys. Rev. Lett.* **1994**, *73*, 3321−3324.
(21) Maher, M. J.; Self, J. L.; Stasiak, P.; Blachut, G.; Ellison, C. J.; Matsen, M. W.; Bates, C. M.; Willson, C. G. Structure, Stability, and Reorganization of 0.5 L0 Topography in Block Copolymer Thin Films. *ACS Nano* **2016**, *10*, 10152−10160.
(22) Samant, S. P.; Grabowski, C. A.; Kisslinger, K.; Yager, K. G.; Yuan, G.; Satija, S. K.; Durstock, M. F.; Raghavan, D.; Karim, A. Directed Self-Assembly of Block Copolymers for High Breakdown Strength Polymer Film Capacitors. *ACS Appl. Mater. Interfaces* **2016**, *8*, 7966−7976.
(23) Ye, Y.-S.; Rick, J.; Hwang, B.-J. Ionic Liquid Polymer Electrolytes. *J. Mater. Chem. A* **2013**, *1*, 2719−2743.
(24) Gartner, T. E.; Morris, M. A.; Shelton, C. K.; Dura, J. A.; Epps, T. H. Quantifying Lithium Salt and Polymer Density Distributions in Nanostructured Ion-Conducting Block Polymers. *Macromolecules* **2018**, *51*, 1917−1926.
(25) Zhang, S.; Lee, K. H.; Frisbie, C. D.; Lodge, T. P. Ionic Conductivity, Capacitance, and Viscoelastic Properties of Block Copolymer-Based Ion Gels. *Macromolecules* **2011**, *44*, 940−949.
(26) Bennett, T. M.; Pei, K.; Cheng, H.-H.; Thurecht, K. J.; Jack, K. S.; Blakey, I. Can Ionic Liquid Additives Be Used to Extend the Scope of Poly(Styrene)-Block-Poly(Methyl Methacrylate) for Directed Self-Assembly? *J. Micro/Nanolithogr., MEMS, MOEMS* **2014**, *13*, No. 031304.
(27) Virgili, J. M.; Nedoma, A. J.; Segalman, R. A.; Balsara, N. P. Ionic Liquid Distribution in Ordered Block Copolymer Solutions. *Macromolecules* **2010**, *43*, 3750−3756.
(28) Chen, X.; Zhou, C.; Chen, S.-J.; Craig, G. S. W.; Rincon-Delgadillo, P.; Dazai, T.; Miyagi, K.; Maehashi, T.; Yamazaki, A.; Gronheid, R.; Stoykovich, M. P.; Nealey, P. F.; et al. Ionic Liquids as Additives to Polystyrene-b-Poly (Methyl Methacrylate) Enabling Directed Self-Assembly of Patterns with Sub-10 Nm Features. *ACS Appl. Mater. Interfaces* **2018**, *10*, 16747−16759.
(29) Yamamuro, O.; Someya, T.; Kofu, M.; Ueki, T.; Ueno, K.; Watanabe, M. Heat Capacities and Glass Transitions of Ion Gels. *J. Phys. Chem. B* **2012**, *116*, 10935−10940.
(30) Zhang, X.; Douglas, J. F.; Satija, S.; Karim, A. Enhanced Vertical Ordering of Block Copolymer Films by Tuning Molecular RSC Advances Enhanced Vertical Ordering of Block Copolymer Fi Lms by Tuning Molecular Mass. *RSC Adv.* **2015**, *5*, 32307−32318.
(31) Ye, C.; Sun, Y.; Karim, A.; Vogt, B. D. Extending Dynamic Range of Block Copolymer Ordering with Rotational Cold Zone Annealing (RCZA) and Ionic Liquids. *Macromolecules* **2015**, *48*, 7567−7573.
(32) Wang, J. Y.; Chen, W.; Roy, C.; Sievert, J. D.; Russell, T. P. Influence of Ionic Complexes on Phase Behavior of Polystyrene-b-Poly(Methyl Methacrylate) Copolymers. *Macromolecules* **2008**, *41*, 963−969.
(33) Earle, M. J.; Esperanca, J. M.S.S.; Gilea, M. A.; Canongia Lopes, J. N.; Rebelo, L. P.N.; Magee, J. W.; Seddon, K. R.; Widegren, J. A. The Distillation and Volatility of Ionic Liquids. *Nature* **2006**, *439*, 831−834.
(34) Fragiadakis, D.; Dou, S.; Colby, R. H.; Runt, J. Molecular Mobility and Li+ Conduction in Polyester Copolymer Ionomers Based on Poly(Ethylene Oxide). *J. Chem. Phys.* **2009**, *130*, No. 064907.
(35) This Article Identifies Certain Commercial Materials, Equipment, or Instruments to Specify Experimental Procedures. Such Identification Implies Neither Recommendation or Endorsement by the National Institute of Standards and Technology.
(36) Jiang, Z. GIXSGUI: A MATLAB Toolbox for Grazing-Incidence X-ray Scattering Data Visualization and Reduction, and Indexing of Buried Three-Dimensional Periodic Nanostructured Films. *J. Appl. Crystallogr.* **2015**, *48*, 917−926.
(37) Kienzle, P. A.; O'Donovan, K. V.; Ankner, J. F.; Berk, N. F.; Majkrzak, C. F. *NCNR Reflectometry Software*.
(38) Russell, T. P.; Coulon, G.; Deline, V. R.; Miller, D. C. Characteristics of the Surface-Induced Orientation for Symmetric Diblock PS/PMMA Copolymers. *Macromolecules* **1989**, *22*, 4600−4606.
(39) Coulon, G.; Russell, T. P.; Deline, V. R.; Green, P. F. Surface-Induced Orientation of Symmetric, Diblock Copolymers: A Secondary Ion Mass Spectrometry Study. *Macromolecules* **1989**, *22*, 2581−2589.
(40) Longanecker, M.; Modi, A.; Dobrynin, A.; Kim, S.; Yuan, G.; Jones, R.; Satija, S.; Bang, J.; Karim, A. Reduced Domain Size and Interfacial Width in Fast Ordering Nanofilled Block Copolymer Films by Direct Immersion Annealing. *Macromolecules* **2016**, *49*, 8563−8571.
(41) Fetters, L. J.; Lohse, D. J.; Richter, D.; Witten, T. A.; Zirkel, A. Connection between Polymer Molecular Weight, Density, Chain Dimensions, and Melt Viscoelastic Properties. *Macromolecules* **1994**, *27*, 4639−4647.
(42) Liu, Y.; Rafailovich, M. H.; Sokolov, J.; Schwarz, S. A.; Bahal, S. Effects of Surface Tension on the Dislocation Structures of Diblock Copolymers. *Macromolecules* **1996**, *29*, 899−906.
(43) Samant, S.; Basutkar, M.; Singh, M.; Masud, A.; Grabowski, C. A.; Kisslinger, K.; Strzalka, J.; Yuan, G.; Satija, S.; Apata, I.; Raghavan, D.; Durstock, M.; Karim, A.; et al. Effect of Molecular Weight and Layer Thickness on the Dielectric Breakdown Strength of Neat and Homopolymer Swollen Lamellar Block Copolymer Films. *ACS Appl. Polym. Mater.* **2020**, *2*, 3072−3083.
(44) Ruiz, R.; Bosworth, J. K.; Black, C. T. Effect of Structural Anisotropy on the Coarsening Kinetics of Diblock Copolymer Striped Patterns. *Phys. Rev. B: Condens. Matter Mater. Phys.* **2008**, *77*, 1−5.
(45) Lambooy, P.; Russell, T. P.; Kellogg, G. J.; Mayes, A. M.; Gallagher, P. D.; Satija, S. K. Observed Frustration in Confined Block Copolymers. *Phys. Rev. Lett.* **1994**, *72*, 2899−2902.
(46) RamachandraRao, V. S.; Gupta, R. R.; Russell, T. P.; Watkins, J. J. Enhancement of Diblock Copolymer Ordering Kinetics by Supercritical Carbon Dioxide Annealing. *Macromolecules* **2001**, *34*, 7923−7925.
(47) Bhadauriya, S.; Wang, X.; Nallapaneni, A.; Masud, A.; Wang, Z.; Lee, J.; Bockstaller, M. R.; Al-Enizi, A. M.; Camp Jr, C. H.; Stafford, C. M.; Douglas, J. F.; Karim, A.; et al. Observation of General Entropy−Enthalpy Compensation Effect in the Relaxation of Wrinkled Polymer Nanocomposite Films. *Nano Lett.* **2021**, 1274.
(48) Kim, S.; Bates, C. M.; Thio, A.; Cushen, J. D.; Ellison, C. J.; Willson, C. G.; Bates, F. S. Consequences of Surface Neutralization in Diblock Copolymer Thin Films. *ACS Nano* **2013**, *7*, 9905−9919.

https://doi.org/10.1021/acs.macromol.0c02546
Macromolecules 2021, 54, 4531−4545

(49) Bang, J.; Bae, J.; Löwenhielm, P.; Spiessberger, C.; Given-Beck, S. A.; Russell, T. P.; Hawker, C. J. Facile Routes to Patterned Surface Neutralization Layers for Block Copolymer Lithography. *Adv. Mater.* **2007**, *19*, 4552−4557.
(50) Koneripalli, N.; Singh, N.; Levicky, R.; Bates, F. S.; Gallagher, P. D.; Satija, S. K. Confined Block Copolymer Thin Films. *Macromolecules* **1995**, *28*, 2897−2904.
(51) Stasiak, P.; McGraw, J. D.; Dalnoki-Veress, K.; Matsen, M. W. Step Edges in Thin Films of Lamellar-Forming Diblock Copolymer. *Macromolecules* **2012**, *45*, 9531−9538.
(52) Anastasiadis, S. H.; Russell, T. P.; Satija, S. K.; Majkrzak, C. F. Neutron Reflectivity Studies of the Surface-Induced Ordering of Diblock Copolymer Films. *Phys. Rev. Lett.* **1989**, *62*, 1852−1855.
(53) Anastasiadis, S. H.; Russell, T. P.; Satija, S. K.; Majkrzak, C. F. The Morphology of Symmetric Diblock Copolymers as Revealed by Neutron Reflectivity. *J. Chem. Phys.* **1990**, *92*, 5677−5691.
(54) Helfand, E.; Tagami, Y. Theory of the Interface between Immiscible Polymers. II. *J. Chem. Phys.* **1972**, *56*, 3592−3601.
(55) Bennett, T. M.; Jack, K. S.; Thurecht, K. J.; Blakey, I. Perturbation of the Experimental Phase Diagram of a Diblock Copolymer by Blending with an Ionic Liquid. *Macromolecules* **2016**, *49*, 205−214.
(56) Hayirlioglu, A.; Kulkarni, M.; Singh, G.; Al-Enizi, A. M.; Zvonkina, I.; Karim, A. Block copolymer ordering on elastomeric substrates of tunable surface energy. *Emergent Mater.* **2019**, *2*, 11−22.

https://doi.org/10.1021/acs.macromol.0c02546
Macromolecules 2021, 54, 4531−4545